Journal Name

ARTICLE TYPE

Cite this: DOI: 10.1039/xxxxxxxxxx

Functional liquid structures by emulsification of graphene and other two-dimensional nanomaterials

Matthew J. Large,[a*] Sean P. Ogilvie,[a] Manuela Meloni,[a] Aline Amorim Graf,[a] Giuseppe Fratta,[a] Jonathan Salvage,[b] Alice A. K. King,[a] and Alan B. Dalton[a*]

Received Date
Accepted Date

DOI: 10.1039/xxxxxxxxxx

www.rsc.org/journalname

Pickering emulsions stabilised with nanomaterials provide routes to a range of functional macroscopic assemblies. We demonstrate the formation and properties of water-in-oil emulsions prepared through liquid-phase exfoliation of graphene. Due to the functional nature of the stabiliser, the emulsions exhibit conductivity due to inter-particle tunnelling. We demonstrate a strain sensing application with a large gauge factor of ∼40; the highest reported in a liquid. Our methodology can be applied to other two-dimensional layered materials opening up applications such as energy storage materials, and flexible and printable electronics.

The interesting functional properties of many two-dimensional (2D) materials are often only observed when the particles are in their mono- or few-layer forms. Such properties include the widely reported, and extremely large, electrical and thermal conductivity of graphene[1], for example, or the direct-bandgap semiconductor behaviour of transition metal dichalcogenides (TMDs)[2]. Strong inter-particle dispersion forces must be overcome in order to exfoliate these nanomaterials, and they also drive aggregation of the isolated particles. Reaggregation has been a long-standing roadblock to utilisation of nanomaterials in macroscopic materials systems on industrially-relevant scales.

Emulsification of nanomaterials is an effective method for formation of macroscopic structures while preserving the degree of particle exfoliation, facilitating the formation of self-assembled liquid structures with functional properties. Pickering emulsions were first described in detail by S.U. Pickering in a 1907 paper[3] on oil-in-water emulsions stabilised by precipitated salt nanoparticles. More recently, clays have been used to stabilise oil-in-water emulsions[4] as well as polymerisation reactions[5]. Such solid-stabilised emulsions are understood to have several advantages over typical surfactant-stabilised emulsions[6]; the structures of these two systems are illustrated in Figure 1**a-b**. Due to the much greater free energy decrease associated with adsorption of the solid particles at the liquid-liquid interface, Pickering emulsions are extremely stable (both over time and with elevated temperature) and are not susceptible to spontaneous phase separation[3].

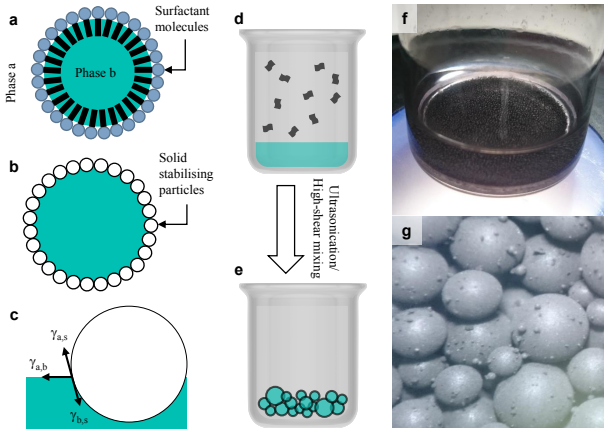

Fig. 1 a: Standard oil-in-water emulsion stabilised by amphiphilic surfactant molecules. **b**: Pickering oil-in-water emulsion stabilised by solid particles. **c**: Illustration of the interfacial tension components at the three-phase boundary in a Pickering emulsion system. **d-e**: Illustration of the formation process for layered nanomaterial-stabilised water-in-oil Pickering emulsions. A dispersion of nanoparticles in the matrix phase is added to the droplet phase to be emulsified; the mixture is subsequently homogenised. **f-g**: Photograph and optical microscope image of the formed droplets in a water-in-oil emulsion stabilised with pristine graphene.

In this paper, we discuss the use of 2D nanomaterials as stabilisers for water-oil emulsions, where the nanomaterial of choice confers additional system functionality. We demonstrate a sensor where liquid-exfoliated graphene acts as both stabiliser and conductive filler. This approach may be built upon to produce

[a] *University of Sussex, Falmer, Brighton, BN1 9RH, United Kingdom. E-mail: m.large@sussex.ac.uk; a.b.dalton@sussex.ac.uk*
[b] *Image Analysis Unit, University of Brighton, Brighton, BN2 4GJ, United Kingdom.*
† Electronic Supplementary Information (ESI) available: Materials, experimental methods, and characterisation of graphene platelets. See DOI: 10.1039/b000000x/

functional structures for a range of other applications, such as energy storage materials for supercapacitors and batteries; water filtration, purification and pumping (by electro-osmosis); wearable, flexible and printable electronics, to name but a few.

The necessary condition for Pickering emulsion formation is that both immiscible phases partially wet the stabiliser surface[6]. Equivalently, one must ensure the two spreading coefficients S, for liquids a and b, on the solid surface have the same sign;

$$S_a = \gamma_{a,s} - \gamma_{b,s} - \gamma_{a,b},$$

$$S_b = \gamma_{b,s} - \gamma_{a,s} - \gamma_{a,b} \quad (1)$$

The three interfacial tensions $\gamma_{a,b}$ (liquid-liquid), $\gamma_{a,s}$ and $\gamma_{b,s}$ (solid-liquid) dictate which phase will form the matrix (more negative S, corresponding to a higher affinity for the stabiliser), and which will form the droplets (greater S). This interfacial force balance is illustrated in Figure 1**c**. It should be noted that the surface tension of the stabilising solid must necessarily be between those of the liquids in order to form an emulsion. Conveniently, graphene and similar 2D materials are understood to have surface tensions in between water and water-immiscible liquids.

Figure 1**d** and **e** schematically illustrate the formation of a nanomaterial-stabilised emulsion. To demonstrate the simplicity of the process, we use deionised water and a common household oil (baby oil, which is primarily paraffin or mineral oil) to prepare Pickering emulsions stabilised with layered materials. Initially graphite is ultrasonically exfoliated into the oil phase to yield a dispersion of multilayer graphene nanoparticles with a modal thickness of $\sim$10 nm (see Supplementary Information). This dispersion is then homogenised after addition of water, first by shaking and subsequently by brief ultrasonic mixing. Following coalescence of the initially formed droplets an equilibrium size distribution is rapidly reached by Ostwald ripening. Figure 1**f** and **g** shows a photograph and optical micrograph (respectively) of such an emulsion. These systems remain stable over several months.

To understand the structures in Figure 1**f** and **g** we calculate the spreading coefficients using an interfacial tension approximation[7];

$$\gamma_{a,b} = \gamma_a + \gamma_b - 4\frac{\gamma_a\gamma_b}{\gamma_a + \gamma_b} \quad (2)$$

where γ_a and γ_b are the surface tensions of the respective phases. For the liquids the surface tensions are readily characterised experimentally, with $\gamma_{oil} = 28.0\,\mathrm{mN\,m^{-1}}$ and $\gamma_{water} = 72.2\,\mathrm{mN\,m^{-1}}$. However, for 2D materials there is a larger degree of uncertainty surrounding the correct value[8]; for example, the surface tension of graphene is estimated to be in the range of 40 to 50 $\mathrm{mN\,m^{-1}}$ [9–11]. Taking the suggested value $\gamma_{graphene} = 40\,\mathrm{mN\,m^{-1}}$ [12] with the given values for the liquids we find that $S_{oil} = -28\,\mathrm{mN\,m^{-1}}$ and $S_{water} = -16\,\mathrm{mN\,m^{-1}}$; this model correctly describes that water forms the droplet phase in the stable Pickering emulsion. Calculations suggest that low surface tension organic liquids are capable of forming similar water-in-oil emulsions; such as n-hexane ($\gamma = 18.8\,\mathrm{mN\,m^{-1}}$), ethyl acetate ($\gamma = 23.2\,\mathrm{mN\,m^{-1}}$), and cyclopentanone ($\gamma = 33.3\,\mathrm{mN\,m^{-1}}$).

The fact that the surface tension of graphene is between those of water and many common water-immiscible liquids is convenient. This is necessary for the formation of stable emulsions, and negates the need for surface modification (by functionalisation or the use of surfactants) to control the surface tension of the nanoparticles. Modifications of this kind are well known to compromise the properties of 2D nanomaterials and their assemblies.

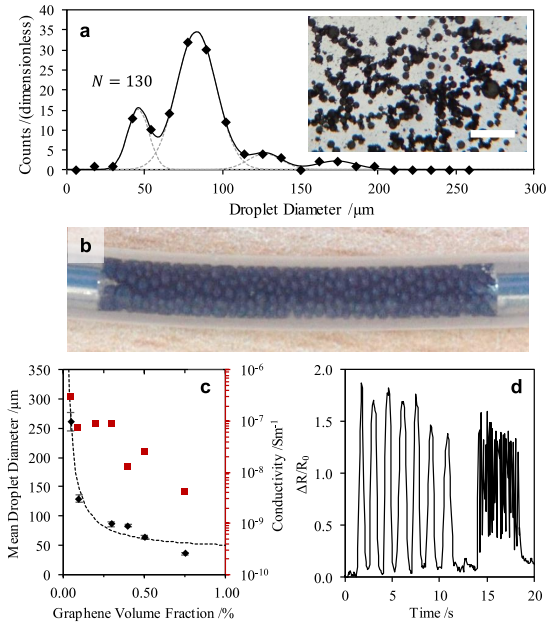

Fig. 2 a: Representative measurement of the emulsion droplet size distribution, with a multimodal Gaussian fit. (inset) optical micrograph of emulsion droplets under bright field illumination (the scale bar is 500 μm). **b**: Photograph of a "liquid wire" formed by encapsulating a graphene emulsion in a silicone pipe. **c**: Measurements of the mean droplet diameter, and emulsion conductivity, as a function of graphene volume fraction. **d**: Fractional resistance change against time for a liquid wire system under repetitive manual strain.

Figure 2**a** shows a representative measurement of the droplet diameter distribution, measured from the inset optical micrograph. The data is fitted using a multimodal Gaussian model. The multiple peaks are due to incomplete interfacial coverage of the initial droplets, which have a characteristic diameter d_i. By coalescence d_i increases (reducing the surface area-to-volume ratio) and thereby drives the system towards stability[13]. The appearance of a multimodal distribution of sizes is therefore indicative that the stabiliser concentration is insufficient to fully stabilise the droplets as they are formed during the homogenisation process.

Using a geometric argument about the interfacial area of the stabiliser (assuming full coverage of the droplets), it can be shown that;

$$d - d_i = \frac{12 V_D N}{V_S \rho_S \mathrm{SSA}} \quad (3)$$

where d [m] is the characteristic droplet diameter; $V_S\rho_S$ [g] is the stabiliser mass (where V_S and ρ_S are the volume and density); SSA [$\mathrm{m^2\,g^{-1}}$] is the stabiliser specific surface area; N is the nominal layer number, and the total droplet volume is V_D [mL]. Clearly the droplet diameter decreases with increasing volume fraction (V_S/V_D) and decreasing layer number of the stabiliser.

We note that if the initially formed droplets (with diameter d_i)

are fully covered by stabiliser then it is not possible for the droplet diameter to decrease further, and any excess stabiliser will remain un-emulsified. Equally, even if there is sufficient stabiliser present in the system the homogenisation procedure will affect the proportion of material that is trapped at the liquid-liquid interface. In the present system the proportion of graphene emulsified is estimated to be at least 90 % based on UV-Visible spectroscopy measurements of the "supernatant" immediately after emulsification and sedimentation of the droplets in a representative sample. Using this measurement we estimate that the fractional surface coverage of the droplets is greater than 1 for all samples described by Figure 2**c**. This suggests that the droplet surfaces are entirely coated with graphene, and that there is a degree of re-aggregation of the stabiliser during the emulsification process.

This type of system acts as a segregated network when the droplets pack together; due to the functional nature of the stabilising material we observe the emergence of system-scale functional properties. In the graphene-stabilised system, electron tunnelling at particle-particle contacts leads to electrical conduction across and between the droplet surfaces and gives rise to macroscopic conductivity across the system. The inherent conductivity of the graphene-oil dispersion prior to emulsification is negligible ($\sim 40\,\mathrm{fS\,m^{-1}}$ at $11.3\,\mathrm{mg\,ml^{-1}}$ graphene, corresponding to 1 vol % at the oil-water ratio used to prepare the emulsions). Based on this we anticipate no significant contribution to the system conductivity as a result of un-emulsified graphene in the oil phase.

Figure 2**b** shows a simple application whereby an emulsion is encapsulated in a silicone pipe with electrical end contacts. The mean droplet diameter, as well as the emulsion conductivity in such pipe structures, are characterised as a function of the volume fraction of the stabilising graphene nanoparticles in Figure 2**c**. The mean droplet diameters are fitted using equation (3).

We immediately notice from Figure 2**c** that the conductivity is correlated with the droplet diameter and inversely correlated with the graphene volume fraction. This unexpected result contrasts with the typical percolation behaviour observed in composites such as latex-nanocarbon systems[14]. This is due to the fact that, in essence, the spheres in the Pickering emulsion system can be considered to have an effective surface conductivity due to near-continuous coverage with the stabilising graphene particles. However, in the latex composite systems the conductive filler is localised exclusively at the interstitial voids between adjacent polymer particles. This means that in our Pickering system the conductivity is dominated by the inter-particle electron tunnelling and the droplet packing. Since the aspect ratio of the stabilising particles is high, a thin oil layer will be maintained between contacting droplets which prevents coalescence (to maintain the three-phase contact at the edges of the stabilising particles). As such electrons experience an additional tunnelling barrier (which is dependent on the dielectric properties of the oil phase) on top of the inter-layer tunnelling barrier present in graphitic multilayers. Since the bulk conductivity in graphite has an anisotropy of ~ 1000 between the directions parallel and perpendicular to the basal plane, we anticipate that the system-scale conductivity is limited by inter-droplet contact resistance. Further, the packing fraction of the droplets (which affects the average coordination number; the average number of neighbours each droplet is in contact with) correlates with the overall conductivity. Both the packing fraction and coordination number increase with the polydispersity of the droplet diameter distribution.

Since tunnelling dominates the electron transport, such devices have a large resistance change with strain (in a similar way to elastomer-based composites[15,16]). Figure 2**d** is a plot of relative resistance change $\Delta R/R_0$ against time under repeated manual strain for the liquid wire shown in Figure 2**b**. The first range shows a strain of approximately 5 % with a frequency of 0.7 Hz, followed by a similar strain with a frequency of 5.3 Hz. As the droplets are deformed under strain transfer from the pipe, their surface area-to-volume ratio increases. Increases in the inter-particle separation on the droplet surface lead to the rapid and reversible rise in resistance observed. There will also be a threshold where non-affine reordering of the droplets minimises the system stress. This may be irreversible and will contribute to drift in the measurements. Based on the approximate amplitudes of the strain and resistance change in Figure 2**d**, the gauge factor of the system shown is ~ 40; the highest reported for a liquid[17]. This is comparable to high-sensitivity elastomer-graphene composites previously described, with gauge factors of up to 35[15]. The system we describe is liquid-based with a simple preparation procedure, with potential for integration into a range of applications.

It is interesting to note that, at the highest graphene mass fraction studied (0.75 vol % or $\sim$1.6 wt %), the effective loading of the system relative to the droplet phase is $16\,\mathrm{mg\,mL^{-1}}$; significantly higher than the maximum stable concentration in many other liquid-phase exfoliation methodologies (in solvents such as NMP $C_{max} \approx 1\,\mathrm{mg\,mL^{-1}}$ [18]; in surfactant-water systems $C_{max} \approx 0.3\,\mathrm{mg\,mL^{-1}}$ [19]). We believe that tailored emulsion systems may be used to produce high-loading inks suitable for printing. In such applications it is important to understand and control the droplet size distribution and droplet volume fraction, since these parameters dominate the emulsion rheology[20,21].

Micro-emulsification techniques can produce droplets with diameters of order 100 nm. Pickering emulsions can be formed with droplet-matrix ratios up to ~ 50 % (where droplet sedimentation/buoyancy can achieve higher volume ratios post-preparation). Therefore it is possible to stabilise $20\,\mathrm{mg\,ml^{-1}}$ of monolayer graphene provided the platelet sizes are small enough to allow conformation to the interface. Typically, liquid exfoliated and size-selected graphene is 3-5 layers thick, which places an upper bound on the mass concentration of 60 to $100\,\mathrm{mg\,ml^{-1}}$, which is comparable to microfluidisation of graphite[22]. Since the surface tension of graphene is similar to graphite[10], we expect our results to be robust to the degree of material exfoliation.

The broad optical absorption of graphene also confers the capability to directly apply energy to the droplets in the form of laser irradiation. This facilitates direct, non-contact manipulation of the droplet contents in microfluidic applications. The Supplementary Multimedia files show laser-induced heating of graphene-stabilised emulsion droplets using a 405 nm laser, with approximately $4\,\mu$W incident radiation per droplet. The localised heat generation forms tight advective flows which drives the droplet movement in the matrix phase, and the emulsion remains stable

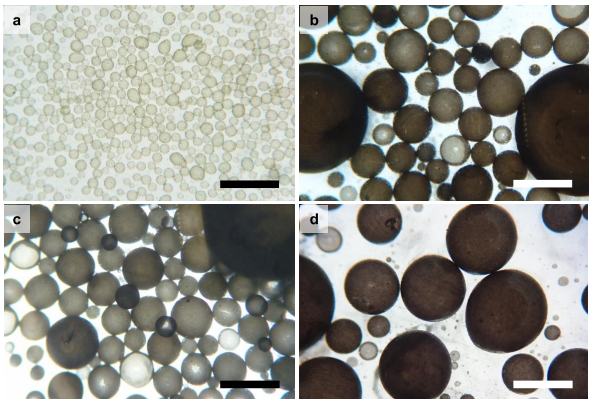

Fig. 3 Optical micrographs of **a** boron nitride, **b** molybdenum disulfide, **c** tungsten disulfide, and **d** molybdenum diselenide-stabilised emulsion droplets under bright field illumination. The scale bars in all cases are 1 mm.

under continuous illumination under these conditions. It is also possible to control the stability of emulsion droplets directly by applying laser radiation in a similar manner[23].

The process used to form these emulsions is not limited to graphene. Figure 3 demonstrates a range of material stabilisers with different properties. This makes use of the fact that the surface tensions of most layered nanomaterials are demonstrably similar[24], and so there is little variation in the spreading coefficients calculated using equations (1) and (2). Figure 3 demonstrates emulsions stabilised with hexagonal boron nitride (h-BN; Figure 3**a**), molybdenum disulfide (MoS_2, Figure 3**b**), tungsten disulfide (WS_2, Figure 3**c**) and molybdenum diselenide ($MoSe_2$, Figure 3**d**). This set of materials, alongside graphene, exhibit conducting, semi-conducting, and insulating behaviours. As such, this system could be used to prepare emulsions with a range of functionalities for applications like high surface area electrode and catalyst structures, functional inks, and microfluidic devices.

In summary, we have demonstrated a simple method, using readily available materials, for preparing functional Pickering emulsion structures stabilised by graphene. The influence of composition on the droplet diameter distribution was studied. The droplets are fully coated with graphene particles, and a degree of re-aggregation is inferred from measurements of the surface coverage. We anticipate that the graphene quality could be improved through a careful choice of liquid phases, however the present results show the possibilities of the most simple realisation.

The electrical properties of this system appear to be dominated by contact resistance between adjacent droplets resulting from electron tunnelling. Making use of this effect, we have demonstrated a strain-sensing application for graphene-stabilised Pickering emulsions which has a gauge factor of ~ 40. This is comparable to other state-of-the-art graphene-based devices[15].

Since the mass concentration in these stabilised systems is very high relative to other liquid stabilisation techniques, Pickering emulsions are an ideal route to producing nanomaterial-carrying inkjet inks. A significant advantage is the ability to control the dispersion viscosity using only the droplet volume fraction[20,21]; this eliminates the need for viscosity modifiers such as poly-(ethylene glycol) which hamper the performance of printed structures using conventionally formulated graphene inks.

We have further shown that the available range of functional properties may be expanded using materials such as boron nitride and transition metal dichalcogenides.

Conflict of interest

There are no conflicts to declare.

Acknowledgements

The authors would like to thank Zenyatta Ventures Ltd for supplying graphite powder. The authors are also grateful to Thomas Swan Ltd for supplying boron nitride powder.

Author contributions

ABD, MJL developed the study concepts. MJL, MM, SO performed experiments. AAG, JS performed SEM imaging. MJL, GF performed Raman spectroscopy. MJL, SPO, ABD prepared the manuscript. SPO, AAKK, ABD reviewed the final manuscript.

References

1 A. K. Geim, *Science*, 2009, **324**, 1530–1534.
2 Q. H. Wang, K. Kalantar-Zadeh, A. Kis, J. N. Coleman and M. S. Strano, *Nature Nanotechnology*, 2012, **7**, 699–712.
3 S. U. Pickering, *Journal of the Chemical Society, Transactions*, 1907, **91**, 2001–2021.
4 N. P. Ashby and B. P. Binks, *Physical Chemistry Chemical Physics*, 2000, **2**, 5640–5646.
5 S. Cauvin, P. J. Colver and S. A. F. Bon, *Macromolecules*, 2005, **38**, 7887–7889.
6 Y. Chevalier and M.-A. Bolzinger, *Colloids and Surfaces A: Physicochemical and Engineering Aspects*, 2013, **439**, 23–34.
7 S. Wu, *Journal of Polymer Science Part C: Polymer Symposia*, 1971, **34**, 19–30.
8 A. Ferguson, A. Harvey, I. J. Godwin, S. D. Bergin and J. N. Coleman, *2D Materials*, 2016, **4**, 015040.
9 Y. Hernandez, V. Nicolosi, M. Lotya, F. M. Blighe, Z. Sun, S. De, I. T. McGovern, B. Holland, M. Byrne, Y. K. Gun'Ko, J. J. Boland, P. Niraj, G. Duesberg, S. Krishnamurthy, R. Goodhue, J. Hutchison, V. Scardaci, A. C. Ferrari and J. N. Coleman, *Nature Nanotechnology*, 2008, **3**, 563–568.
10 S. Wang, Y. Zhang, N. Abidi and L. Cabrales, *Langmuir*, 2009, **25**, 11078–11081.
11 A. Kozbial, Z. Li, C. Conaway, R. McGinley, S. Dhingra, V. Vahdat, F. Zhou, B. D'Urso, H. Liu and L. Li, *Langmuir*, 2014, **30**, 8598–8606.
12 Y. Hernandez, M. Lotya, D. Rickard, S. D. Bergin and J. N. Coleman, *Langmuir*, 2010, **26**, 3208–3213.
13 T. Wu, H. Wang, B. Jing, F. Liu, P. C. Burns and C. Na, *Nature Communications*, 2015, **6**, 5929.
14 I. Jurewicz, P. Worajittiphon, A. A. K. King, P. J. Sellin, J. L. Keddie and A. B. Dalton, *The Journal of Physical Chemistry B*, 2011, **115**, 6395–6400.
15 C. S. Boland, U. Khan, C. Backes, A. O'Neill, J. McCauley, S. Duane, R. Shanker, Y. Liu, I. Jurewicz, A. B. Dalton and J. N. Coleman, *ACS Nano*, 2014, **8**, 8819–8830.
16 C. S. Boland, U. Khan, G. Ryan, S. Barwich, R. Charifou, A. Harvey, C. Backes, Z. Li, M. S. Ferreira, M. E. Mobius, R. J. Young and J. N. Coleman, *Science*, 2016, **354**, 1257–1260.
17 D. Y. Choi, M. H. Kim, Y. S. Oh, S.-H. Jung, J. H. Jung, H. J. Sung, H. W. Lee and H. M. Lee, *ACS Applied Materials & Interfaces*, 2017, **9**, 1770–1780.
18 U. Khan, A. O'Neill, M. Lotya, S. De and J. N. Coleman, *Small*, 2010, **6**, 864–871.
19 M. Lotya, P. J. King, U. Khan, S. De and J. N. Coleman, *ACS Nano*, 2010, **4**, 3155–3162.
20 W. H. Cogill, *Nature*, 1965, **207**, 742–743.
21 R. Pal, *Journal of Rheology*, 2001, **45**, 509–520.
22 P. G. Karagiannidis, S. A. Hodge, L. Lombardi, F. Tomarchio, N. Decorde, S. Milana, I. Goykhman, Y. Su, S. V. Mesite, D. N. Johnstone, R. K. Leary, P. A. Midgley, N. M. Pugno, F. Torrisi and A. C. Ferrari, *ACS Nano*, 2017, **11**, 2742–2755.
23 M. D. J. Quinn, K. Vu, S. Madden and S. M. Notley, *ACS Applied Materials & Interfaces*, 2016, **8**, 10609–10616.
24 J. N. Coleman, M. Lotya, A. O'Neill, S. D. Bergin, P. J. King, U. Khan, K. Young, A. Gaucher, S. De, R. J. Smith, I. V. Shvets, S. K. Arora, G. Stanton, H.-Y. Kim, K. Lee, G. T. Kim, G. S. Duesberg, T. Hallam, J. J. Boland, J. J. Wang, J. F. Donegan, J. C. Grunlan, G. Moriarty, A. Shmeliov, R. J. Nicholls, J. M. Perkins, E. M. Grieveson, K. Theuwissen, D. W. McComb, P. D. Nellist and V. Nicolosi, *Science*, 2011, **331**, 568–571.

Functional liquid structures by emulsification of graphene and other two-dimensional nanomaterials

Matthew J. Large[1,*], Sean Ogilvie[1], Manuela Meloni[1], Aline Amorim Graf[1], Giuseppe Fratta[1], Jonathan Salvage[2], Alice King[1], and Alan B. Dalton[1,*]

[1]University of Sussex, Falmer, Brighton, BN1 9RH, United Kingdom
[2]Image Analysis Unit, University of Brighton, Brighton, BN2 4GJ, United Kingdom
[*]m.large@sussex.ac.uk; a.b.dalton@sussex.ac.uk

Supporting Information

1 Materials and methods

1.1 Materials

Graphite powder (supplied by Zenyatta Ventures Ltd) with a nominal 3.5 µm particle size was used as-received. Hexagonal boron nitride powder (supplied by Thomas Swan Ltd), which had been prepared according to [1] in surfactant solution and subsequently dried and washed, was used as-received. MoS_2, $MoSe_2$, and WS_2 powders were purchased from Sigma Aldrich. These sieved powders (with 1 to 2 µm particle sizes) were used as-received. A commercially available brand of baby oil was purchased and used as-received; the primary constituent is paraffin oil. Type 1 purified water (18.2 MΩ cm resistivity) was prepared in-house using a Thermo Scientific MicroPure filtration system.

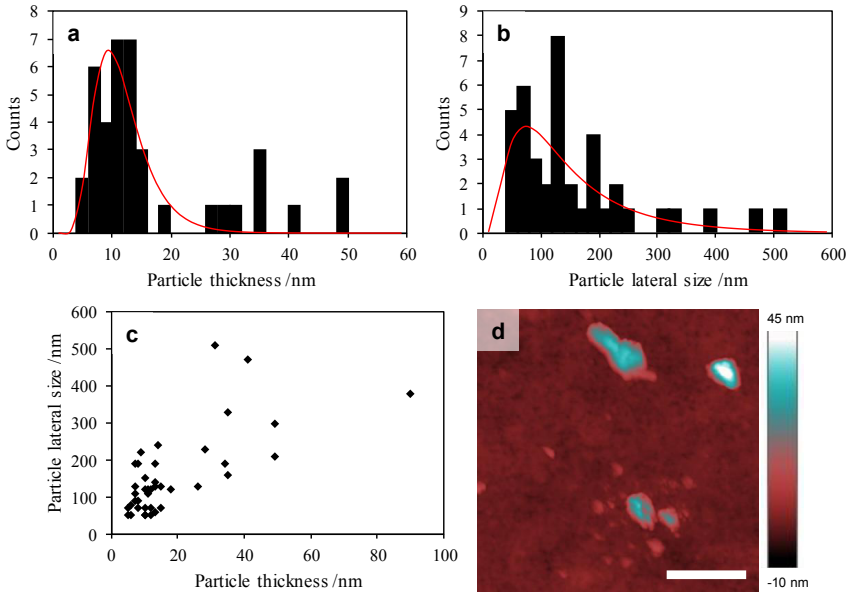

Figure S1: **a**: Histogram of exfoliated graphene particle thicknesses measured by AFM. The sample mean is 18 nm, and the mean of the fitted lognormal distribution is 12 nm. The sample also contained a small number of partially-exfoliated crystallites (since no size selection steps were used) with thicknesses in the range of 200 to 500 nm. **b**: Histogram of particle lateral sizes. Both the sample mean and mean of the fitted lognormal distribution is 160 nm. **c**: Plot of particle lateral size against particle thickness, indicating a weak positive correlation. **d**: Representative AFM height image (the scale bar is 500 nm).

1.2 Procedures

The surface tensions of the liquids used were characterised using the Wilhelmy plate method using a Nima PS4 surface pressure sensor.

To form water-in-oil emulsions, the nanomaterial powders were first ultrasonically exfoliated into the oil phase. Sonication was performed using a Sonics Vibracell VCX750 probe sonicator with output pulsing (6 s on, 2 s off) and 60 % tip amplitude (∼45 W power) for 3 hours. The sonicated dispersion was further diluted with oil to achieve the desired volume (mass) fraction of the stabiliser relative to constant volumes of the oil and water phases (preserving the total sample volume in all cases).

A sample of the exfoliated material on glass was prepared by rod-coating

of the oil dispersion, followed by rinsing with hexane to remove residual oil from the surface. AFM imaging was performed using a Bruker Dimension Icon microscope operating in Peak Force Tapping Mode. Four fields were captured across the sample to yield a representative distribution of particle sizes (see Figure S1).

A sample of the exfoliated material was further characterised by Raman spectroscopy and scanning electron microscopy (SEM), alongside a sample of the supplied graphite material (see Figure S2). We observe a shift in the G-band position from 1560 cm^{-1} in the as-received graphite to 1580 cm^{-1}, which is consistent with exfoliated graphene materials. However the intensity ratio of the 2D to G bands indicates that the material is only partially exfoliated (as anticipated from the AFM measurements).

SEM imaging was performed with a Zeiss SIGMA field emission gun scanning electron microscope (FEG-SEM) using a Zeiss in-lens secondary electron detector. The FEG-SEM working conditions used were; 2.5 kV accelerating voltage, 20 µm aperture, and 2 mm working distance.

To prepare the emulsions, water (2 ml) and the diluted oil dispersions (4 ml) were added to hydrophobized glass containers and shaken vigorously for 30 s by hand. This was followed by 60 s of ultrasonic homogenisation using a Sonics Vibracell VCX130 with 30 % tip amplitude and output pulsing (6 s on, 2 s off). Once the emulsions had been homogenised, the droplets were allowed to sediment for several hours. A sample was pipetted to a hydrophobized microscope slide for optical microscopy. The droplet size distribution was measured using ImageJ; 130 measurements were used to compose diameter histograms for each prepared sample.

The emulsion samples were pipetted into silicone pipe (2 mm internal diameter) and sealed with electrical end contacts connected to a Keithley 2614B sourcemeter. I-V characterisation was performed to characterise the electrical behaviour of the samples.

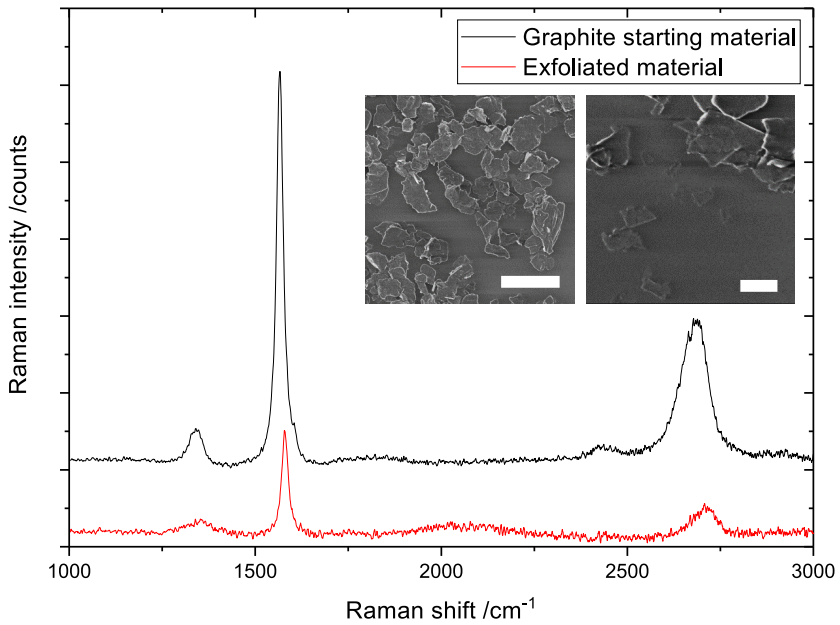

Figure S2: Raman spectra for samples of the supplied graphite and exfoliated nanoparticles. (inset) SEM images corresponding to the two samples; As-received graphite (left, scale bar 4 µm) and exfoliated nanomaterial (right, scale bar 400 nm).

References

[1] K. R. Paton et al. "Scalable Production of Large Quantities of Defect-Free Few-Layer Graphene by Shear Exfoliation in Liquids". In: *Nature Materials* 13.6 (2014), pp. 624–630. DOI: 10.1038/nmat3944.